PERGAMON International Journal of Multiphase Flow 24 (1998) 1025–1055

International Journal of Multiphase Flow

Evaluation of equilibrium and non-equilibrium evaporation models for many-droplet gas-liquid flow simulations

R. S. Miller, K. Harstad, J. Bellan *

Jet Propulsion Laboratory, California Institute of Technology, Pasadena, CA 91109-8099, U.S.A

Received 28 July 1997; received in revised form 7 May 1998

Abstract

A variety of liquid droplet evaporation models, including both classical equilibrium and non-equilibrium Langmuir–Knudsen formulations, are evaluated through comparisons with experiments with particular emphasis on computationally efficient procedures for gas–liquid flow simulations. The models considered are those used in droplet laden flow calculations such as direct numerical simulations for which large numbers of individual (isolated) droplet solutions are obtained. Diameter and temperature evolution predictions are made for single-component droplets of benzene, decane, heptane, hexane and water with relatively large initial sizes $\sim$1 mm vaporizing in convective air flows. All of the models perform nearly identically for low evaporation rates at gas temperatures significantly lower than the boiling temperature. For gas temperatures at and above the boiling point, large deviations are found between the various model predictions. The simulated results reveal that non-equilibrium effects become significant when the initial droplet diameter is $< 50\ \mu$m and that these effects are enhanced with increasing slip velocity. It is additionally observed that constant properties can be used throughout each simulation if both the gas and vapor values are calculated at either the wet-bulb or boiling temperature. The models based on the Langmuir–Knudsen law and a corrected (for evaporation effects) analytical heat transfer expression derived from the quasi-steady gas phase assumption are shown to agree most favorably with a wide variety of experimental results. Since the experimental droplet sizes are all much larger than the limit for non-equilibrium effects to be important, for these conditions the most crucial aspect of the current Langmuir–Knudsen models is the corrected analytical form for the heat transfer expression as compared to empirical relations used in the remaining models.

Keywords: Condensation; Droplet; Evaporation; Non-euilibrium; Spray

* Corresponding author.

PII: S0301-9322(98)00028-7

1. Introduction

A large diversity of multi-phase gas–liquid flows of both scientific and practical interest involve the evaporation (or condensation) of near spherical liquid droplets in high (or low) temperature turbulent environments. Such flows cover a wide range of applications including spray cooling, spray combustion, fire suppression and air–fuel premixing in combustors. All of these situations involve a dispersed liquid phase species in the form of a large number of discrete droplets convecting and vaporizing in a continuous gas phase species, and their mathematical description involves complex nonlinear couplings of momentum, energy and mass exchange. Regardless of the macroscopic complexity of the flow field, the traditional modeling approach for such flows generally involves specifying the governing equations for a single, isolated droplet including drag, convective heat transfer, mass transfer and effects due to finite droplet Reynolds numbers (Sirignano, 1993). The derived equations are then used either for every individual droplet, as in direct numerical simulations, or for a subset of statistically representative droplets ("test particles") as in various forms of two-phase turbulence and spray modeling (e.g. Crowe et al., 1996).

Modern direct numerical simulations currently treat as many as 10^6 individual solid particles undergoing dispersion in simplified turbulent flow configurations (see Eaton and Fessler, 1994 for a related review); however, such massive computations are relatively new for evaporating droplets due to the numerical complexity added by the droplet heat and mass transfer. Mashayek et al. (1997) simulate droplet dispersion in isotropic turbulence for which the evaporation is governed by the classical "D^2 law" (Godsave, 1953; Spalding, 1953a) and the mass loading is considered small enough to neglect turbulence modulation by the dispersed phase (one-way coupling). More recently, Mashayek (1998a) and Mashayek (1998b) removed this restriction and considered droplet dispersion in compressible homogeneous turbulence with two-way coupling and droplet evaporation governed by a heat–mass transfer analogy model first used by Crowe et al. (1977). Their simulations employ 96^3 spectral collocation points for the gas phase discretization and include as many as 5.5×10^5 sets of Lagrangian equations for the three dimensional position, velocity, temperature and mass of each droplet. Stochastic approaches in which only representative droplets are followed have received much wider attention than the direct simulation approach; being less expensive computationally. A complete review of related work is beyond the scope of this paper; however, we refer the reader to Sirignano (1993) for a recent review of Lagrangian spray modeling, to Drew and Lahey (1993) for a review of Eulerian droplet modeling in which the dispersed phase is treated as a stochastic continuum, and to Crowe et al. (1996) for a recent review of general two-phase modeling approaches.

The above discussions clearly illustrate the need for accurate and computationally efficient procedures for evaluating the trajectories and thermodynamic-evaporation evolutions of single droplets for use in large scale gas–liquid flow simulations. Aggarwal et al. (1984) evaluated several evaporation models for stochastic spray simulations, including both constant droplet temperature and transient heating versions of the classical model. They recommend using a spherically symmetric formulation with finite liquid conductivity when the droplet is stationary, and an axisymmetric internal circulation model when the droplet Reynolds number is substantially larger than unity. Unfortunately, neither of these forms is appropriate when many

droplets are involved due to the extreme computational expense of resolving both the droplet interior and exterior boundary layers in either one or two dimensions. Furthermore, this work only compares the evaporation models to each other, with no comparison with either experiments or with more detailed non-equilibrium evaporation models. This method of comparing results obtained with models of increasing complexity, but using the same equilibrium form for the evaporation rate, appears to be the primary means of evaluation found in the literature (e.g. Hubbard et al., 1975; Renksizbulut and Haywood, 1988; Abramzon and Sirignano, 1989). Such an approach cannot distinguish the limitations due to the equilibrium evaporation law included in all of the models (see Aggarwal and Peng, 1995 for a recent review of equilibrium droplet modeling). Bellan and Summerfield (1978) first introduced the non-equilibrium Langmuir–Knudsen evaporation law for use in droplet combustion models and found non-equilibrium effects to be important for droplet sizes found in practical spray calculations. For very small droplet sizes occurring during condensation and nucleation processes, Jackson and Davidson (1983) incorporate the non-equilibrium Herz–Knudsen law (applicable to the free molecule regime) in their Eulerian–Eulerian gas–liquid flow model. Finally, the extent of actual comparisons with experimental measurements even for the traditional classical evaporation model appears to be limited almost entirely to cases of droplet combustion for which the flame temperature and effects of buoyancy must be estimated (e.g. Law and Law, 1976); thus rendering the comparisons uncertain. One very recent exception is by Chen et al. (1997) who compare both infinite and finite liquid conductivity versions of the classical equilibrium model to experiments for decane and hexane droplets $\sim 50\ \mu$m at moderate evaporation rates; however, there are possible inconsistencies in their results as discussed in detail below.

The purpose of the present paper is to perform an evaluation of existing evaporation models which are applicable to modern many-droplet calculations at low pressures. Of particular interest is the vaporization of small hydrocarbon droplets in high temperature environments as found in many spray mixing and spray combustion processes (Sirignano, 1993). The models considered include two versions of the transient classical model, four heat–mass transfer analogy models and two non-equilibrium models based on the Langmuir–Knudsen evaporation law. None of the models require spatial resolution along the droplet coordinate, and therefore only derivatives with respect to time are involved. Efficient methods for evaluating the temperature dependencies of species properties are also discussed. Furthermore, we include detailed comparisons with experimental results for single-component water, benzene, decane, heptane and hexane droplets vaporizing (without combustion) in low, moderate and high temperature air (both quiescent and convecting). The paper is organized as follows: Section 2 describes the formulation and limiting assumptions of the eight different models examined in the paper. Detailed comparisons with experimental results for the droplet surface area and temperature evolutions are provided in Section 3; the relevance of non-equilibrium effects and reference conditions for property evaluations are highlighted. Section 4 provides further discussions and conclusions.

2. Formulation

Consider the case of a two-phase flow in which the dispersed phase is in the form of discrete single-component spherical liquid droplets with density much larger than that of the surrounding ambient gas, and momentum exchange with the carrier gas is assumed to be only a function of the drag force (i.e. Basset history, added mass and other terms are neglected). Furthermore, the thermal energy exchange between phases is assumed to occur only though convective heat transfer, and internal droplet vortical flow is neglected. Under these conditions, the generic Lagrangian equations describing the transient position (X_i), velocity (v_i), temperature (T_d) and mass (m_d) of a single droplet are:

$$\frac{dX_i}{dt} = v_i, \tag{1}$$

$$\frac{dv_i}{dt} = \left(\frac{f_1}{\tau_d}\right)(u_i - v_i) + g_i, \tag{2}$$

$$\frac{dT_d}{dt} = \frac{f_2 Nu}{3Pr_G}\left(\frac{\theta_1}{\tau_d}\right)(T_G - T_d) + \left(\frac{L_V}{C_L}\right)\frac{\dot{m}_d}{m_d} - H_{\Delta T}, \tag{3}$$

$$\frac{dm_d}{dt} = -\frac{Sh}{3Sc_G}\left(\frac{m_d}{\tau_d}\right)H_M, \tag{4}$$

where $\dot{m}_d = dm_d/dt$ is negative for evaporation, u_i and T_G are the local carrier gas velocity and temperature, g_i is gravitational acceleration, L_V is the latent heat of evaporation, the ratio of the gas (constant pressure) heat capacity to that of the liquid phase is $\theta_1 = C_{p,G}/C_L$, and the gas phase Prandtl and Schmidt numbers in terms of the viscosity (μ), thermal conductivity (λ) and binary diffusion coefficient (Γ) are $Pr_G = \mu_G C_{p,G}/\lambda_G$ and $Sc_G = \mu_G/\rho_G\Gamma_G$ (with gas density ρ_G), respectively. The subscripts denote the vector component (i), droplet (d), gas phase property (G) away from the droplet surface, vapor phase of the evaporate (V), and liquid phase (L). In (2)–(4), $\tau_d = \rho_d D^2/(18\mu_G)$ is the particle time constant for Stokes flow, where D is the droplet diameter, and f_1 is a correction to Stokes drag for droplet motion and evaporation. Furthermore, f_2 is a correction to heat transfer due to evaporation, and the Nusselt (Nu) and Sherwood (Sh) numbers are empirically modified for convective corrections to heat and mass transfer, respectively. Finally, $H_{\Delta T}$ represents any additional terms used to incorporate non-uniform internal temperature effects (i.e. finite liquid thermal conductivity), and H_M represents the specific driving potential for mass transfer (analogous to $T_G - T_d$ for heat transfer).

Equations (1)–(4) have been modified from their traditional appearances in order to highlight the differences between models, and also to emphasize the time scale τ_d which is known to play a crucial role in determining the particle dispersion in turbulent flows (e.g. Eaton and Fessler, 1994; Crowe et al., 1996). These equations describe a general class of droplet models used in a variety of studies, each model being identified by specific choices for f_1, f_2, Nu, Sh, $H_{\Delta T}$ and H_M as described below. In this section we introduce eight such evaporation models which differ predominantly through the calculation of the heat and mass transfer terms f_2, H_M and $H_{\Delta T}$. In order to make more meaningful comparisons which

characterize the differences among the model predictions, it is therefore appropriate to choose consistent formulations for the remaining free parameters f_1, Nu and Sh.

Many models have been used to describe deviations from Stokes drag (f_1) in various ranges of slip velocity and/or evaporation rate. Bellan and Harstad (1987b) compared several drag corrections for clusters of evaporating droplets and found little deviation among the simulated results. One example of the empirical drag correction for finite particle Reynolds numbers ($Re_d = \rho_G u_s D/\mu_G$ is related to the slip velocity, and $Re_b = \rho_G u_b D/\mu_G$ is related to the blowing velocity) is:

$$f_1 = \frac{1 + .0545\ Re_d + .1\ Re_d^{\frac{1}{2}}(1 - .03\ Re_d)}{1 + a|Re_b|^b}, \qquad (5)$$

$$a = 0.09 + 0.077\exp(-0.4\ Re_d), \quad b = 0.4 + 0.77\exp(-0.04\ Re_d),$$

where $u_s = |u_i - v_i|$ is the slip velocity magnitude, and u_b is obtained from the relation $\dot{m}_d = -\pi\rho_G D^2 u_b$. Equation (5) is a correlation fit to the numerical results of Cliffe and Lever (1985) over the range $0 \leq Re_d \leq 100$ and $0 \leq Re_b \leq 10$ (Bellan and Harstad, 1987b). Although other correlations have been fit to wider ranges of Re_d (see Aggarwal and Peng, 1995 for a recent review), in most spray calculations involving relatively dense clustering of the droplets, the slip velocity relaxes quickly due to a decrease in the effective ''permeability' of the cluster (Bellan and Harstad, 1987b; Harstad and Bellan, 1991). Equation (5) is fit to very high accuracy and is therefore considered to provide an improved drag correction compared to other relations fit to wider Reynolds number ranges, while being applicable to the flow configurations relevant to this study. For heat and mass transfer, the widely used Ranz Marshall correlations (Ranz and Marshall, 1952a; Ranz and Marshall, 1952b) for the Nusselt and Sherwood numbers:

$$Nu = 2 + 0.552\ Re_d^{\frac{1}{2}} Pr_G^{\frac{1}{3}}, \quad Sh = 2 + 0.552\ Re_d^{\frac{1}{2}} Sc_G^{\frac{1}{3}}, \qquad (6)$$

are chosen for all of the models (see e.g. Sirignano, 1993 for alternative correlations). Note that either of these forms can be used to calculate the Reynolds number modification to the quiescent (subscript q) evaporation rate as suggested by Williams (1965); i.e. $\dot{m}_d = (Nu/2)\ \dot{m}_{d,q} = (Sh/2)\ \dot{m}_{d,q}$, for unity Lewis number.

Eight different models are selected for comparisons as presented in Table 1. Nomenclature is as follows: Y is the vapor mass fraction (Y_G refers to the free stream vapor mass fraction away from the droplet surface), $\theta_2 = W_C/W_V$ is the ratio of molecular weights where subscript C refers to the carrier gas species, and the equilibrium (subscript eq) and non-equilibrium (subscript neq) Spalding transfer numbers for mass (B_M) are defined as

$$B_{M,eq} = \frac{Y_{s,eq} - Y_G}{1 - Y_{s,eq}}, \quad B_{M,neq} = \frac{Y_{s,neq} - Y_G}{1 - Y_{s,neq}}, \qquad (7)$$

respectively, while the transfer number for energy (B_T) is

Table 1
Expressions for the evaporation correction (f_2), internal temperature gradient correction ($H_{\Delta T}$) and mass transfer potential (H_M) from various models

Model	Name	f_2	$H_{\Delta T}$	H_M
M1	Classical rapid mixing†	1	0	$\ln[1 + B_{M,eq}]$
M2	Abramzon–Sirignano†	$\frac{-\dot{m}_d}{m_d B'_T}\left[\frac{3Pr_G\tau_d}{Nu}\right]$	0	$\ln[1 + B_{M,eq}]$
M3	Mass analogy Ia	1	0	$B_{M,eq}$
M4	Mass analogy Ib	$(1 + B_T)^{-1}$	0	$B_{M,eq}$
M5	Mass analogy IIa	1	0	$(Y_{s,eq} - Y_G)$
M6	Mass analogy IIb	$(1 + B_T)^{-1}$	0	$(Y_{s,eq} - Y_G)$
M7	Langmuir–Knudsen I	G	0	$\ln[1 + B_{M,neq}]$
M8	Langmuir–Knudsen II*	G	$\frac{2\beta}{3Pr_G}\left(\frac{\theta_1}{\tau_d}\right)\Delta_s$	$\ln[1 + B_{M,neq}]$

†Properties are evaluated using the "1/3" rule for reference mass fraction.
*An additional equation for $\Delta_s = T_{d,s} - T_d$ is required.

$$B_T = (T_G - T_d)\frac{C_{p,V}}{L_V}. \tag{8}$$

Each of the models requires the knowledge of the mass fraction of the vapor at the droplet surface. This is obtained for models M1–M6 using the equilibrium assumption

$$Y_{s,eq} = \frac{\chi_{s,eq}}{\chi_{s,eq} + (1 - \chi_{s,eq})\theta_2}, \tag{9}$$

where the surface equilibrium mole fraction of the vapor ($\chi_{s,eq}$) is related to the saturation pressure P_{sat} through the Clausius–Clapeyron equation (for constant latent heat)

$$\chi_{s,eq} = \frac{P_{sat}}{P_G} = \frac{P_{atm}}{P_G}\exp\left[\frac{L_V}{\bar{R}/W_V}\left(\frac{1}{T_B} - \frac{1}{T_d}\right)\right], \tag{10}$$

where T_B is the liquid phase normal boiling temperature and $\bar{R}$ is the universal gas constant. Non-equilibrium surface mass fractions are used for the Langmuir–Knudsen models (M7 and M8) as described below.

The following discussion provides a brief description of the various models. Additional details related to the specific derivations and assumptions used in each model may be found in the cited literature. The classical evaporation model (model M1) was first derived by Godsave (1953) and Spalding (1953a) and has received the most attention since its introduction over 40 years ago. This model, also referred to as the "D^2 law", was originally derived assuming a constant droplet temperature fixed at the wet bulb condition, and included the quasi-steady assumption for the gas phase leading to the logarithmic form for the mass transfer potential, H_M (see Table 1). Since its introduction, the importance of transient droplet heating has been recognized (Hubbard et al., 1975), and the evaporation rate is now generally coupled with a time dependent energy equation typically with assumed infinite thermal conductivity of the liquid (e.g. Aggarwal et al., 1984; Chen and Periera, 1996). In this form, the classical model is generally referred to as either the infinite conductivity model, or the rapid mixing model (Aggarwal et al., 1984). We examine the rapid mixing model without evaporation (Stefan flow)

corrections to heat transfer ($f_2 = 1$) as it is most commonly applied in modern spray calculations (e.g. Chen and Periera, 1996).

Abramzon and Sirignano (1989) revised the infinite conductivity model to incorporate the effects of Stefan flow on heat and mass transfer (model M2). In their model, heat transfer is modified through the use of modified forms for the Nusselt, Sherwood and transfer numbers:

$$B'_{\mathrm{T}} = (1 + B_{\mathrm{M,eq}})^{\phi} - 1, \quad \phi = \frac{C_{\mathrm{p,V}}}{\bar{C}_{\mathrm{p}}} \frac{Sh^*}{Nu^*} \frac{1}{\overline{Le}}, \tag{11}$$

$$Nu^* = 2 + \frac{Nu - 2}{F_{\mathrm{T}}}, \quad F_{\mathrm{T}} = \frac{(1 + B'_{\mathrm{T}})^{0.7}}{B'_{\mathrm{T}}} \ln(1 + B'_{\mathrm{T}}), \tag{12}$$

$$Sh^* = 2 + \frac{Sh - 2}{F_{\mathrm{M}}}, \quad F_{\mathrm{M}} = \frac{(1 + B_{\mathrm{M,eq}})^{0.7}}{B_{\mathrm{M,eq}}} \ln(1 + B_{\mathrm{M,eq}}), \tag{13}$$

where the overbar denotes properties that are evaluated using reference conditions for temperature and species concentration as discussed below. The modified Nusselt and Sherwood numbers are substituted for the ordinary forms in (3)–(4) and in Table 1. This model must be solved iteratively for $B_{\mathrm{T}}{}'$ which may be costly for many-droplet simulations. Note that the bracketed term in f_2 (Table 1) cancels with a complementary term in (3) and the convective heat transfer term in the droplet energy equation reduces to $-(\theta_1/m_{\mathrm{d}})(\dot{m}_{\mathrm{d}}/B_{\mathrm{T}}{}')(T_{\mathrm{G}} - T_{\mathrm{d}})$. Recent comparisons between the rapid mixing model and the Abramzon–Sirignano model applied to many-droplet spray calculations suggest that agreement with experimental results is improved using the latter formulation (Chen and Periera, 1996).

Models M3–M6 are all variations of a basic heat–mass transfer analogy model which can be derived directly from the vapor mass fraction boundary condition at the surface of the droplet:

$$\rho_{\mathrm{G,s}} \pi D^2 u_{\mathrm{b}} = \rho_{\mathrm{G,s}} \pi D^2 u_{\mathrm{b}} Y_{\mathrm{s}} - \rho_{\mathrm{G,s}} \pi D^2 \Gamma_{\mathrm{G}} \left. \frac{\partial Y}{\partial r} \right|_{r=D/2}, \tag{14}$$

where the droplet is assumed to be insoluble to the gas phase species. Model M3 is obtained by simply substituting the surface mass fraction gradient in (14) in terms of the Sherwood number, the droplet diameter and the mass fraction difference, and then utilizing the relationship between u_{b} and $\dot{m}_{\mathrm{d}}$ to yield an equation for the evaporation rate. If first order (linear) corrections for heat transfer due to blowing [$f_2 = (1 + B_{\mathrm{T}})^{-1}$; as discussed in detail below] are incorporated into the energy equation, then model M4 is obtained. Although the heat–mass transfer analogy models do not incorporate the typical quasi-steady logarithmic gas phase profiles, they nevertheless implicitly assume quasi-steadiness due to the time independent Nusselt and Sherwood numbers. Finally, models M5 and M6 are completely analogous to models M3 and M4 except that the denominator $(1 - Y_{\mathrm{s}})$ from $B_{\mathrm{M,eq}}$ (see Table 1) has been assumed to be constant and approximately equal to unity, and absorbed into the definition of Sh, thus making the formulation strictly valid only for very small evaporation rates. In fact, Bird et al. (1960) derive this relation for analysis of mass diffusion through a porous wall and not for phase change phenomena. Note that retention of $(1 - Y_{\mathrm{s}})$ as a denominator ensures that $\dot{m}_{\mathrm{d}} \to -\infty$ as $Y_{\mathrm{s}} \to 1$, thus providing feedback and preventing the droplet from becoming superheated. Models M5 and M6 do not incorporate this effect and can therefore lead to both

$T_d > T_{sat}$ and $Y_s > 1$, where T_{sat} is the pressure dependent saturation temperature (as will be shown below). Nevertheless, these latter models are used for droplet evaporation simulations due to their compact formulation and direct analogy to the energy equation. For example, Crowe et al. (1977) applied the mass analogy model M6 to the problem of a steady two-dimensional cooling spray, while Mashayek (1998a) and Mashayek (1998b) used the same evaporation model for direct numerical simulations of as many as 5.5×10^5 droplets evaporating in homogeneous turbulence (note that both applications involve only $T_G < T_{sat}$ and therefore do not violate the physical droplet temperature constraints described above). To the authors' knowledge, models M3 and M4 have not appeared in the literature; however, they represent less restrictive versions of models M5 and M6 and are therefore included in this study for completeness.

Both models M7 and M8 incorporate a non-equilibrium evaporation law and are therefore expected to be valid under a wider range of conditions than the previous models. Bellan and Harstad (1987a) introduced a droplet evaporation model based on the Langmuir–Knudsen law which also incorporates droplet temperature non-uniformity; the drop temperature is obtained by solving Lagrangian equations for both the droplet surface temperature and the volume averaged internal temperature. In the current paper, we consider both infinite liquid conductivity (M7) and the original finite liquid conductivity (M8) versions of the model. In both cases, the non-equilibrium Langmuir–Knudsen law is incorporated through the definition of the vapor mole fraction at the droplet surface ($\chi_{s,neq}$)

$$\chi_{s,neq} = \chi_{s,eq} - \left(\frac{L_K}{D/2}\right)\beta, \tag{15}$$

where $\chi_{s,eq}$ is defined by (10), L_K is the Knudsen layer thickness

$$L_K = \frac{\mu_G \sqrt{2\pi T_d \bar{R}/W_V}}{\alpha_e Sc_G P_G}, \tag{16}$$

α_e is the molecular accommodation coefficient (assumed equal to unity), and the non-dimensional evaporation parameter (β) is

$$\beta = -\left(\frac{3Pr_G \tau_d}{2}\right)\frac{\dot{m}_d}{m_d}. \tag{17}$$

Note that using the definition of τ_d and u_b reveals that the evaporation parameter is directly proportional to the blowing Reynolds number: $\beta = Pr_G Re_b/2$ (i.e. one half the blowing Peclet number). Finally, the non-equilibrium vapor surface mass fraction is calculated directly from the mole fraction (15).

$$Y_{s,neq} = \frac{\chi_{s,neq}}{\chi_{s,neq} + (1 - \chi_{s,neq})\theta_2}. \tag{18}$$

Note that the surface mole fraction deviates from equilibrium conditions by the product of the evaporation parameter and the Knudsen thickness normalized by the droplet radius, and reduces to (9) as $L_K\beta/D \rightarrow 0$.

A wide variety of Nusselt number correlations have been proposed which incorporate evaporation effects of the type corresponding to the function f_2 in (3). Spalding (1953b) originally suggests using $f_2 = B_T^{-2/5}$. Several other efforts are based on the general form $f_2 = (1 + B_T)^{-\kappa}$: both Eisenklam et al. (1967) and Yuen and Chen (1978) propose the linear form ($\kappa = 1$), while Narashimhan and Gauvin (1967), and Renksizbulut and Yuen (1983) suggest non-linear forms having $\kappa = 2/3$ and $\kappa = 0.7$, respectively. A more complex formulation is given by Downing (1966) for which $f_2 = \{1-0.4[1- B_T^{-1} \ln(1 + B_T)]\}B_T^{-1} \ln(1 + B_T)$. The overall complexity (and/or non-linearity) of the correlations depends on the range of evaporation rates used to correlate the data, and no accepted agreement on the "correct" model has been reached. However, such empirical curve fits are not necessary because the quasi-steady solution of the gas field equations coupled to the drop surface boundary conditions leads directly to an analytic expression for heat transfer reduction due to evaporation; i.e. $f_2 = G$, where

$$G = \frac{\beta}{e^{\beta} - 1}, \tag{19}$$

which is used for both of the non-equilibrium Langmuir–Knudsen models, M7 and M8 (see Table 1). Note that this formulation can be applied for zero evaporation rate using the limit $G \rightarrow 1$ as $\beta \rightarrow 0$. It is interesting to note that this form for heat transfer reduction has very rarely been used with other evaporation models, even though it is a natural extension of the quasi-steady gas phase solution (aside from related discussions in Bird et al., 1960, we are only aware of one study by Berlemont et al., 1991 who use $f_2 = G$ without comment in studying droplet–turbulence interactions with a k–ϵ model). A comparison of all of the available heat transfer corrections is beyond the scope of this paper; therefore, only the most commonly used forms for f_2 listed in Table 1 are included in this study.

Finally, model M8 is derived to include the effects of conduction limited heat transfer within the liquid droplet in a computationally efficient manner. Through extensive operator algebra, Bellan and Harstad (1987a) incorporate these effects into the thermodynamic description with the addition of an equation for the temperature difference, $\Delta_s = T_{d,s} - T_d$ (for this model T_d is the volume averaged droplet temperature governed by (3)):

$$\frac{d\Delta_s}{dt} = -\frac{\theta_3}{Pr_G}\left(\frac{\theta_1}{\tau_d}\right)[5\Delta_s - \alpha^*], \tag{20}$$

where $\theta_3 = \lambda_G/\lambda_L$ and

$$\alpha^* = \theta_3\left[\left(\frac{NuG}{2}\right)(T_G - T_{d,s}) - \left(\frac{L_V}{C_{p,G}}\right)\beta\right]. \tag{21}$$

In this case, the complete internal temperature profile can be reconstructed (to fourth order) as:

$$T(r^*) = T_d - \frac{3}{8}(9\Delta_s - \alpha^*) + \frac{5}{4}(7\Delta_s - \alpha^*)(r^*)^2 - \frac{7}{8}(5\Delta_s - \alpha^*)(r^*)^4, \tag{22}$$

where $r^* = r/R$ is the normalized internal droplet radius. Note that (22) is superfluous to the evaporation evolution prediction of model M8, and is not used in the present study. The model presented originally by Bellan and Harstad (1987a) is more complex than that presented here due to the retention of the $(r^*)^6$ term of the expansion in (22). However, extensive testing performed here shows that the fourth order expansion of (22) provides nearly identical accuracy with a much simplified formulation. Initial conditions for the droplet temperature are not obvious, as uniform internal temperature is not permissible because the model is formulated using the quasi-steady assumption under which the internal droplet temperature is "pre-relaxed." However, a choice of $\Delta_s(t = 0) = 0.06\alpha^*$ is obtained through a least mean square error procedure for the integral of $\partial T/\partial r$ and yields a relatively smooth initial profile. Note that model M8 provides a solution for the droplet surface temperature $T_{d,s}$, and this value should be substituted for T_d in the temperature difference $T_G - T_d$ appearing in (3).

The above discussions provide formulations for each of the eight droplet evaporation models considered in this study. All of the model solutions involve (1)–(4) together with the corresponding expressions for f_2, $H_{\Delta T}$ and H_M provided in Table 1, as well as the expressions for the drag coefficient (5), the Nusselt and Sherwood numbers, (6), and the transfer numbers, (7) and (8), (except for model M2 which uses (11)–(13)). All of the equilibrium models (M1–M6) specify the droplet surface vapor mass fraction using (9) and (10), whereas non-equilibrium effects are incorporated into models M7 and M8 using (15)–(18). Finally, model M8 requires the solution of an additional droplet energy equation given by (20) and (21). Additionally, the ideal gas equation of state is used to calculate both the vapor and carrier gas densities as functions of specified temperatures and pressures.

2.1. Properties

Implicit in the derivations of all of the models described above is the assumption that the gas and vapor properties are constant in space, and therefore independent of the temperature (see Law and Law, 1976 for a discussion). Thus, for physical consistency, these models must be based on characteristic average constant property values that accurately account for the real spatial and thermal property variations. Unfortunately, several past studies have shown that evaporation rate predictions are sensitive to the choice of property values (e.g. Kassoy and Williams, 1968; Law and Law, 1976). The general approach is to define reference values for the temperature (T_R) and the vapor mass fraction (Y_R) which are used to evaluate both the gas and vapor properties:

$$T_R = T_{d,s} + A(T_G - T_{d,s}), \quad Y_R = Y_s + A(Y_G - Y_s), \tag{23}$$

where the coefficient $0 \leq A \leq 1$ determines the relative contribution of the surface and far field conditions. Initially, Law and Williams (1972) proposed the value A = 1/2, while more recently Yuen and Chen (1976) recommended $A = 1/3$ corresponding to the well known "1/3 rule"; this latter value has gained a more general acceptance (e.g. Hubbard et al., 1975). Given the vapor and gas properties evaluated at the reference temperature, the corresponding mixture values are then calculated at the reference mass fraction using an appropriate mixture averaging

procedure. For example, the semi-empirical Wilke rule is often used for the diffusive properties (Reid et al., 1987). For a binary mixture, this relation states that:

$$\bar{\Phi} = \frac{\chi_R \Phi_V}{\chi_R + (1-\chi_R)\Omega_{VG}} + \frac{(1-\chi_R)\Phi_G}{\chi_R \Omega_{GV} + (1-\chi_R)}, \tag{24}$$

$$\Omega_{ab} = \frac{\{1 + \Phi_a/\Phi_b)^{\frac{1}{2}}(W_b/W_a)^{\frac{1}{4}}\}^2}{\{8(1+W_a/W_b)\}^{\frac{1}{2}}}, \tag{25}$$

where Φ denotes μ, λ or Γ, and the reference mole fraction (χ_R) is calculated from Y_R in (23). Also for a binary mixture, a linear mass averaging of the constant pressure, gas phase heat capacity yields:

$$\overline{C_p} = Y_R C_{p,V} + (1 - Y_R) C_{p,G}. \tag{26}$$

These property evaluations are generally used at each numerical time step and can add significant computational expense when many droplets are involved.

For the purpose of this study, we choose an alternative approach in which the properties are evaluated only once, at the beginning of each simulation, based on the estimated wet bulb temperature (T_{WB}); T_{WB} is essentially the steady state surface temperature achieved during evaporation (Yuen and Chen, 1976; also illustrated below). This approach assumes (only for the purpose of property evaluation) that the droplet surface temperature is quickly raised from initial conditions to the wet bulb value and that this surface temperature is the appropriate condition for evaluating both the vapor and carrier gas properties. The pure air free stream considered in this paper does not require any mixture calculations of the type in (23)–(26), as the models have been formulated in terms of only the far field gas or the pure vapor properties (except for models M1 and M2 as described below). It will be shown that this method is relatively successful for the conditions considered in this study and has the added advantage of significantly reducing the computational expense due to property evaluations.

Lacking an accurate theoretical means by which to calculate the wet bulb temperature, we employ an empirical correlation to experimental results for a variety of fuels. A correlation for T_{WB} as a function of the free stream temperature and the liquid boiling point:

$$T_{WB} = 137\left(\frac{T_B}{373.15}\right)^{0.68} \log_{10}(T_G) - 45, \tag{27}$$

is fit in the present study to experimental values for the particular fuels used here (temperatures in degrees Kelvin). Fig. 1 shows that the correlation is valid over a wide range of temperatures for all fuels; however, caution is warranted before using this relation for un-tested species or for different pressures. In addition, we still employ the time dependent "1/3 rule" in terms of reference mass fraction for both the rapid mixing and the Abramzon–Sirignano models (M1 and M2) in order to be consistent with common applications of these models. The effects of this approach and other reference conditions will be discussed in more detail below where it will be shown that using the boiling temperature also yields reasonable results; the advantage

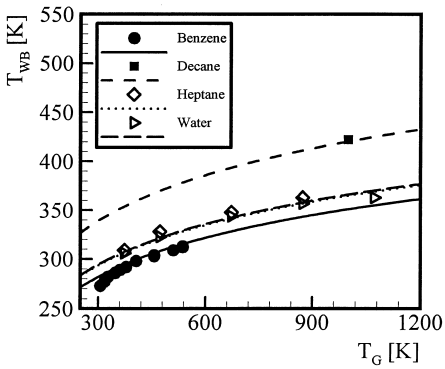

Fig. 1. Comparison of experimental wet bulb measurements with the correlation described by (27). The experimental data is from Yuen and Chen (1976) for water and heptane; the data for decane is from Wong and Lin (1992); and from Downing (1966) for benzene.

of using T_B instead of T_{WB} is that estimates of T_{WB} are not generally available. All necessary property correlations used in this study are provided in the Appendix.

3. Results

For the purpose of this study, it is desirable to evaluate the evaporation models through comparisons with single droplet vaporization (without combustion) experiments for small hydrocarbon droplets ($\sim 10\ \mu m \rightarrow 100\ \mu m$) in high temperature ($T_G > 1000$ K) convective gas environments, as found in many practical spray applications (Sirignano, 1993). Recent advances in non-intrusive optical techniques have made highly accurate measurements of small droplet evaporation evolutions possible (Chen et al., 1996). Swindal et al. (1996) implement this technique and state a sensitivity of 1 nm in droplet radius change for a fuel droplet with a radius of 40 μm; however, the results are for closely spaced droplet streams with low gas temperature, and are therefore not applicable to the present study. Chen et al. (1997) present both experimental results and model predictions corresponding to decane and hexane droplets with initial diameters between 55 and 65 μm, injected through a moderate temperature air flow having relatively strong temperature and velocity gradients. Attempts made during the course of this investigation to compare the present model predictions with these experiments were unsuccessful for reasons which will be discussed at the end of this section. Temperature measurements of substantially larger hexadecane droplets (283 μm) in free fall were obtained by Hanlon and Melton (1992) with a moderate gas temperature equal to 773 K; in this case the elapsed measurement time is small (120 ms) and the droplet diameter is actually observed to increase by several percent during this period (explained as being due to thermal expansion effects). Similar temperature results were obtained by Wells and Melton (1990) for 225 μm decane droplets falling freely in a low temperature nitrogen environment at 473 K. These experiments are also for relatively low evaporation rates and no droplet size measurements are provided. Unfortunately, the extent of experimental data which is applicable to the present study appears to be limited to relatively large droplet sizes $\sim$1 mm as described below, and we

could not find equivalent experimental data for small droplet sizes to use for our model evaluations.

The above models are evaluated to determine the accuracy and range of validity of each model, with particular emphasis on droplet size and temperature evolutions. All results are for single, isolated droplets evaporating in an infinite, constant temperature and constant velocity ($u_i = U_G$) air environment which is assumed to be unaltered by the droplet presence. In order to simplify the comparisons, all simulations conform to an experimental situation in which the droplet remains stationary (hanging from the end of a thin wire) such that (1) and (2) are superfluous and the gas phase velocity only appears in the definition of the Reynolds number. Detailed comparisons with experimental results are made for low, moderate and high evaporation rates as determined by the gas temperature relative to the boiling point of the liquid species; including water, benzene, decane, heptane and hexane. All results presented in this paper are for ambient pressures equal to one standard atmosphere (note that in this case $T_B = T_{sat}$).

Numerical solutions of the governing equations for each evaporation model are obtained using a fourth order accurate, four stage Runge–Kutta discretization of the temporal derivatives. Although the resulting Langmuir–Knudsen relation ((4) for models M7 and M8) is written implicitly for β (i.e. $\dot{m}_d$), it is not necessary to solve this equation iteratively; thorough testing shows that it is always sufficient to use the previous time step value on the right hand side of the equation because of the logarithmic form used here (this presentation is unique to the authors' knowledge). The reason for this is because the non-equilibrium contribution (from the term $2L_K\beta/D$ in (15) which yields the implicit functionality) is generally relatively small for large droplets at atmospheric pressure ($L_K \sim 10^{-7}$ m for water at the boiling temperature). Furthermore, even for small droplets in which the non-equilibrium contribution is significant (as will be shown below), β remains, in general, a relatively slowly varying parameter and is constant for droplets which obey the classical "D^2 law", since (17) and the definition of τ_d yield:

$$\beta = -\left(\frac{\rho_d Pr_G}{8\mu_G}\right)\frac{dD^2}{dt}. \tag{28}$$

Therefore, all of the results reported below are obtained without iteration for β, except for the initial conditions for which the solution generally converges to an accuracy of 10^{-10} with ≈ 5 iterations. In comparison, the Abramzon–Sirignano model M2 requires an iterative procedure for B_T', albeit the actual convergence is relatively rapid and generally requires < 10 cycles at each time step. Furthermore, unless otherwise noted, all temperature results obtained with the finite liquid conductivity model M8 correspond to the surface temperature, $T_{d,s}$ (although it is the volume averaged temperature T_d of (3) which is matched to experimental initial conditions).

3.1. Low, moderate and high evaporation rate comparisons

The performance of each model for relatively low evaporation rates is highlighted in Fig. 2 which depicts the temporal evolutions of the relative surface area and temperature for a single

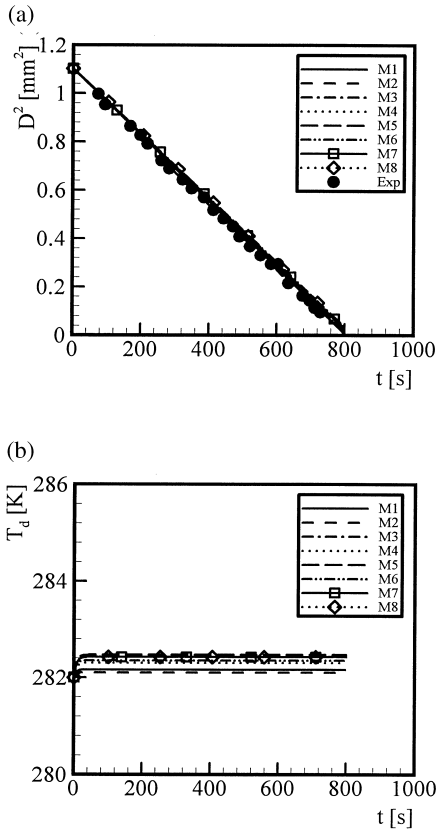

Fig. 2. Temporal evolution of the (a) droplet diameter squared and (b) the droplet temperature for water. The experimental results are from Ranz and Marshall (1952b) and the conditions are: $T_G = 298$ K, $T_{d,0} = 282$ K, $D_0 = 1.1$ mm and $Re_d = 0$.

isolated water droplet ($D_0 = 1.1$ mm and $T_{d,0} = 282$ K) evaporating in a quiescent air environment at $T_G = 298$ K. The model predictions for D^2 are compared to the experimental results of Ranz and Marshall (1952b) obtained under the same conditions. Note that here the droplet Reynolds number is zero and the empirical convective contributions to both the Nusselt and Sherwood numbers are irrelevant. For this relatively low evaporation rate, Fig. 2(a) shows that all of the models predict nearly identical evaporation histories ($\beta \approx 6 \times 10^{-3}$) and that they agree with the experiments. Furthermore, the temperature evolution predictions are also nearly identical for all models [Fig. 2(b)]. Note that the initial droplet temperature is approximately equal to the predicted wet bulb condition resulting in the nearly constant temperature curves. The reason for the observed convergence in model predictions is due to the relatively low gas temperature (which is substantially lower than T_B of water) inducing very small evaporation rates. An examination of the terms appearing in Table 1 in the limit of very small $\dot{m}_d$ (β) shows that all of the mathematical expressions for f_2 approach unity; while all expressions for H_M approach $B_{M,eq}$ as determined by a Taylor expansion. These results show that for large initial droplet diameters and low evaporation rates, the differences between the models are negligible; they all yield the same "D^2 law" behavior observed in the experiments.

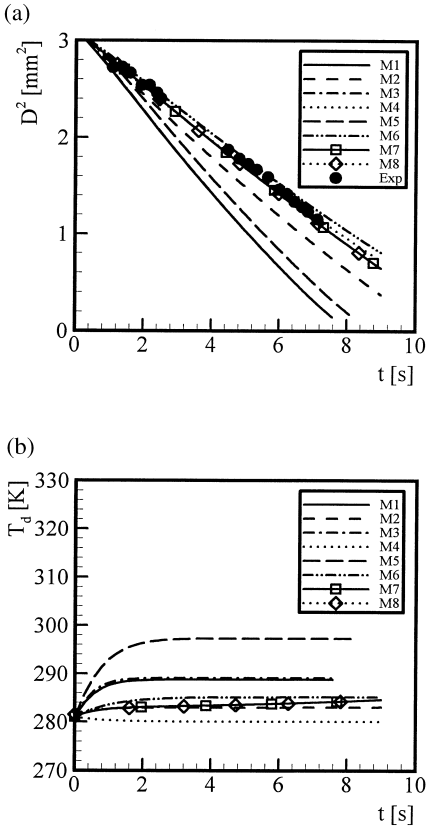

Fig. 3. Temporal evolution of the (a) droplet diameter squared and (b) the droplet temperature for hexane ($T_B = 344.6$ K). The experimental results are from Downing (1966) and the conditions are: $T_G = 437$ K, $T_{d,0} = 281$ K, $D_0 = 1.76$ mm and $Re_{d,0} = 110$.

Variations among the model predictions emerge when the evaporation rate is increased as portrayed by the results of Fig. 3. Here, the time dependent droplet surface area and temperature are compared to the experiments of Downing (1966) for a moderate evaporation rate. The simulations correspond to hexane with an initial droplet size and temperature of $D_0 = 1.76$ mm and $T_{d,0} = 281$ K, suspended in a convective flow with a relatively large initial droplet Reynolds number of $Re_{d,0} = 110$, for which the gas temperature, $T_G = 437$ K, is nearly one hundred degrees above the liquid boiling point. As with the previous results for water, the initial droplet temperature is close to the steady state wet bulb condition. Such initial conditions remove any substantial early transient heat up behavior which may result in deviations from "D^2 law" diameter reduction. This is observed in Fig. 3(a) which shows that all models predict near linear reductions for D^2 with time ($\beta \approx 0.8$ for model M7). The observed linear surface area reduction is also supported by the experimental results. However, unlike the low evaporation rate predictions, the models now yield different rates of diameter decrease. The rapid mixing model M1, the Abramzon–Sirignano model M2 and the mass analogy model M5 all reveal a substantial over prediction in the evaporation rate. Note that the Abramzon–Sirignano model represents, however, a significant improvement over the

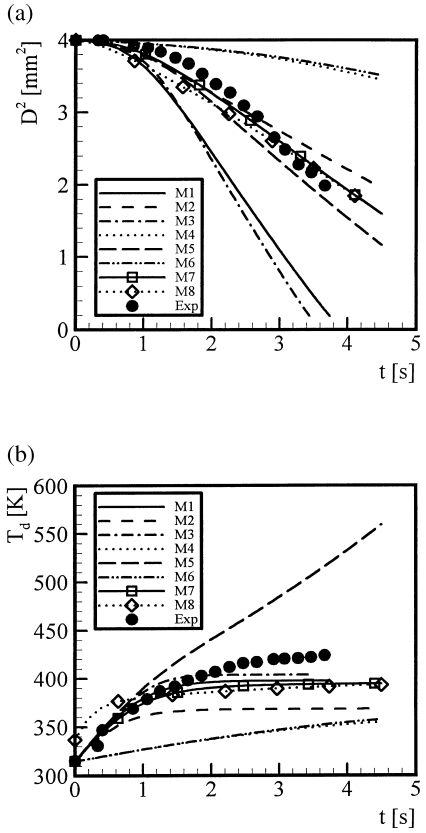

Fig. 4. Temporal evolution of the (a) droplet diameter squared and (b) the droplet temperature for decane ($T_B = 447.7$ K). The experimental results are from Wong and Lin (1992) and the conditions are: $T_G = 1000$ K, $T_{d,0} = 315$ K, $D_0 = 2.0$ mm and $Re_{d,0} = 17$.

standard rapid mixing model which it was meant to correct. The remaining models all predict the experimental data within reasonable accuracy over the entire range for which the results are available; the two non-equilibrium models show nearly identical predictions. The temperature curves in Fig. 3(b) reveal that all models predict droplet temperatures that quickly reach steady state values, and that the relative deviation between these values is in no case larger than approximately 6%. The experiments of Downing (1966) do not include temperature measurements and it is therefore not possible to determine which model most accurately predicts the droplet temperature.

Recent experiments performed by Wong and Lin (1992) provide measurements of both the droplet size and temperature evolutions, allowing for an accurate comparison of the model predictions under conditions of relatively high evaporation rate. Their experiment consists of a droplet of decane with initial size $D_0 \approx 2$ mm and temperature $T_{d,0} = 315$ K placed in a high temperature [$T_G = 1000$ K, greater than twice the liquid boiling temperature ($T_B = 447.7$ K)] convective air stream ($Re_{d,0} = 17$). Furthermore, fine thermocouples placed inside the droplets measure both time and spatially dependent droplet temperatures. Comparisons with the model predictions are provided in Fig. 4 for both the diameter squared and the experimentally

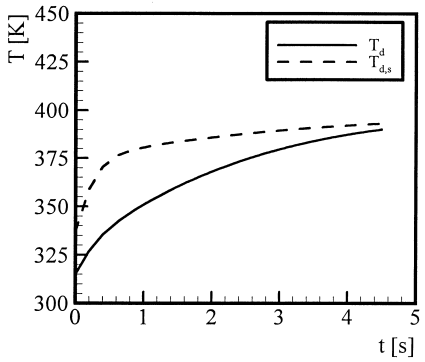

Fig. 5. Temporal evolution of the volume averaged droplet temperature T_d and the surface temperature $T_{d,s}$ calculated from the finite liquid conductivity Langmuir–Knudsen model (M8) for the conditions of Fig. 4.

obtained temperature measured at a fixed droplet radial position corresponding to $r^* = 0.6$. Fig. 4(a) clearly reveals that the relatively large $T_G - T_{d,0}$ results in a strong initial heat up transient stage during which the "D^2 law" is invalid, followed by the classical linear D^2 temporal reduction regime (with $\beta \approx 1.6$ for model M7). The combination of the heat up period and the relatively high evaporation rates results in large discrepancies between the model predictions for both the surface area and the droplet temperature developments. The results illustrated in Fig. 4(a) suggest that the droplet size is best modeled using either of the two non-equilibrium models (M7 and M8), both of which provide nearly identical results. Both the Abramzon–Sirignano model (M2) and the modified mass analogy model (M5) with no heat transfer correction ($f_2 = 1$) also make reasonable size reduction predictions; however, their corresponding temperature predictions [Fig. 4(b)] are substantially lower than, and unphysically larger than the experimental results, respectively. The possibility of having such unphysical over predictions of the droplet temperature, larger than the liquid boiling point, was discussed in Section 2: the two mass analogy models which absorbed the denominator $(1 - Y_s)$ in the analytical mass potential term (H_M) cannot correctly drive the evaporation rate towards infinite values as the droplet temperature approaches the boiling condition and the surface mass fraction approaches unity. This results in the monotonically increasing T_d curve for model M5 in Fig. 4(b). The complementary model M6 which also absorbs this denominator but treats evaporative heat transfer reduction through $f_2 = (1 + B_T)^{-1}$, provides sufficient indirect feed back to avoid this occurrence; however, the droplet temperature is in this case largely underpredicted.

A review of the results of Fig. 4 reveals that the two non-equilibrium models (M7 and M8) provide the best predictions of both the droplet size and temperature evolutions. Note, however, that the finite conductivity model M8 overpredicts the early time droplet temperature due to the inability to specify uniform initial internal droplet temperature profiles as discussed in Section 2. This effect is illustrated in Fig. 5 which shows the predictions of model M8 for both the volume averaged temperature and the droplet surface temperature evolutions corresponding to the results of Fig. 4. The physical nature of the internal droplet temperature "eigenfunctions" from (22) cause the initial profile to portray a small pre-heated region near the droplet surface when there is an imposed external temperature gradient. As heating

commences, the surface temperature increases rapidly for early times. Finally, at later times ($t > 2\,s$) both the volume averaged and surface values converge as the internal temperature reaches a nearly uniform state. The experiments of Wong and Lin (1992) do provide several internal temperature profiles for this case; however, at these droplet Reynolds numbers there is a strong internal vortex motion present and the profiles are characterized by a minimum point near the half radius of the drop. Since the finite conductivity model M8 does not incorporate internal circulation effects, it cannot predict such profiles and therefore no full radial comparisons with (22) are made in this paper.

3.2. Steady state droplet temperature comparisons

Past studies consider that it is sufficient to predict the correct droplet evaporation rate, whereas correct prediction of the droplet temperature is a largely unaddressed issue. However, if the predicted droplet temperature is in error for a spray with a large mass loading, this may introduce a source of substantial errors in the overall flow predictions because of the large thermal inertia of the dispersed phase. In order to further explore the accuracy of droplet temperature predictions, it is valuable to compare the modeled steady state droplet temperatures with experimental measurements of wet bulb temperatures for a variety of fuels. Such comparisons are provided in Fig. 6 for water, benzene and heptane as a function of the far field gas temperature; each curve in the figures corresponds to the results of 25 simulations. In all cases, the steady state droplet temperatures are given at a time when the droplet mass has decreased to 0.1 $m_{d,0}$. The model simulations do not correspond to the actual experimental conditions [Yuen and Chen (1976) use freely falling droplets of unspecified size, but state that the measured steady state droplet temperatures are equal to the wet-bulb conditions] and are characterized by $T_{d,0} = 300$ K, $D_0 = 1$ mm and $Re_d = 0$; however, the steady state temperatures are relatively insensitive to these parameters (insensitivity to Re_d results from the steady states being measured at long times when the droplet size and Re_d are substantially reduced from their initial values: in fact, no steady state is reached until Re_d becomes small). Fig. 6(c) shows that the modified mass analogy model M5 again results in droplet temperatures much larger than the boiling point for large gas temperatures, and can be dismissed for general usage on physical grounds (the inflection point is due to numerically restraining the surface mass fraction from taking values larger than unity).

Of all the models considered in this paper, the two non-equilibrium models (M7 and M8) provide the best overall agreement for the droplet steady state temperatures depicted in Fig. 6; however, all of the models under predict the wet bulb for all but the very lowest gas temperatures (lowest evaporation rates). These under predictions can be explained by examining the energy equation, (3): when the droplet temperature is lumped as in (3), the thermal energy entering the droplet is used to uniformly heat the entire drop ($m_d C_l T_d$). In reality, this energy only heats some fraction of the total mass corresponding to the surface region of the droplet such that a thin thermal boundary layer is formed within the liquid on the inner side of the surface (e.g. Tong and Sirignano, 1982). Therefore, when a substantial internal thermal boundary layer region is established, it is no longer valid to treat the droplet in a lumped temperature manner; droplet temperature non-uniformities of this type must be considered if very accurate droplet temperature predictions are sought. Note that model M8

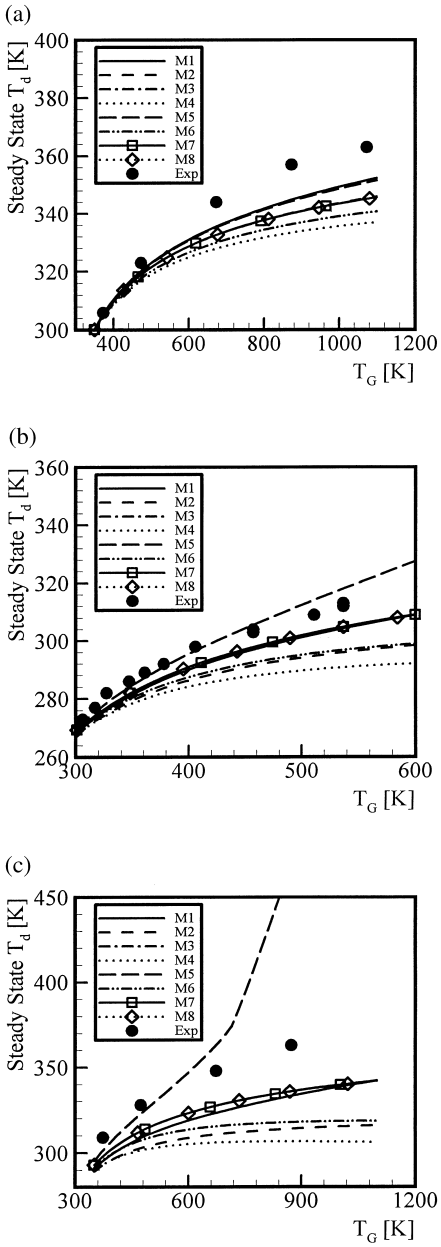

Fig. 6. Comparison of steady state droplet temperatures (measured when $m_d = 0.1\, m_{d,0}$) as a function of the free stream temperature predicted by the models with the experimentally measured wet bulb temperatures for: (a) water (Yuen and Chen, 1976); (b) benzene (Downing, 1966); and (c) heptane (Yuen and Chen, 1976). The conditions are: $T_{d,0} = 300$ K, $D_0 = 1$ mm and $U_G = 0$.

does address internal temperature non-uniformities but retains the lumped temperature heating of $m_d C_l T_d$ (T_d is the volume averaged temperature) in the transient temperature term of (3) (in this sense model M8 may be considered to be thermally "quasi-lumped")

3.3. Thermodynamic non-equilibrium and evaporative heat transfer effects

The improved performance observed for the Langmuir–Knudsen evaporation models (M7 and M8) raises the question of how significant thermodynamic non-equilibrium effects are for the conditions of interest in this study. This question is addressed in Fig. 7 which shows the percent relative non-equilibrium contribution from the term $2L_K\beta/D$ to the surface mole fraction, $\chi_{s,neq}$, defined by (15). The results are given as a function of the initial droplet size [Fig. 7(a)], the gas temperature [Fig. 7(b)] and the convective droplet Reynolds number [Fig. 7(c)], for base case conditions corresponding to the decane experiments of Wong and Lin (1992). As the figure clearly shows, non-equilibrium effects are important for small *initial* droplet sizes $< 50\ \mu$m (for an initial 10 μm diameter droplet, the non-equilibrium contribution ranges from approximately 20% to 80% of the surface mole fraction during the course of evaporation). This diameter range is precisely that of practical sprays used in combustion applications (Sirignano, 1993), but much smaller than that of available experimental measurements for single droplets. The ambient gas temperature [Fig. 7(b)] primarily affects the total evaporation time, and has little influence on non-equilibrium effects for the current droplet parameters. Fig. 7(c) reveals that, for sufficiently small initial droplet sizes, the convective Reynolds number can significantly influence the extent of non-equilibrium behavior by directly increasing the evaporation parameter β. Note that the use of a more volatile fuel will result in a similar enhancement of β due to increased evaporation rates (not shown). The results in Fig. 7(b) and (c) are performed for relatively large droplet sizes to match the baseline experimental data; however, additional testing shows that the observed qualitative trends are retained for small droplet sizes (not shown). The results of Fig. 7 show that non-equilibrium effects are negligible for the large droplets for which the model predictions were validated in Figs. 2–4 and 6, and hence do not explain the previously described improved predictions attributed to the two Langmuir–Knudsen based models (M7 and M8).

Consider the model comparisons presented in Fig. 4 for the decane droplet evaporation. In this case, the maximum contribution of non-equilibrium effects is less than 0.3% over the entire droplet lifetime [Fig. 7(c)]; yet the non-equilibrium models M7 and M8 outperform all of the other models. An examination of the model differences in Table 1 reveals that the only unique attribute of these two models (other than being non-equilibrium) is in the form of the heat transfer correction for evaporation, $f_2 = G$. In order to test the influence of this parameter, the model comparisons with the decane experiments are repeated in Fig. 8 for the identical conditions used previously in Fig. 4; however, for all models we now use the analytic $f_2 = G$ heat transfer correction (curves for M7 and M8 are unchanged). In this case, all of the model predictions are greatly improved (despite a slight deterioration in temperature predictions for models M1 and M3) as compared to the experimental data. Note that differences between the results of models M1 and M7 in Fig. 8(b) are due to the "1/3 rule" reference mass fraction used in M1, and not to non-equilibrium effects which are insignificant for these conditions (see Fig. 7). The modified mass analogy model (M5) results very closely follow the temperature measurements and are within acceptable accuracy for the diameter reduction (though the poorest relative to the other models). However, for the sake of consistency, the quasi-steady profile should be used for both the heat transfer term and for the mass transfer potential, H_M, instead of only for heat transfer (as occurs for model M5 in

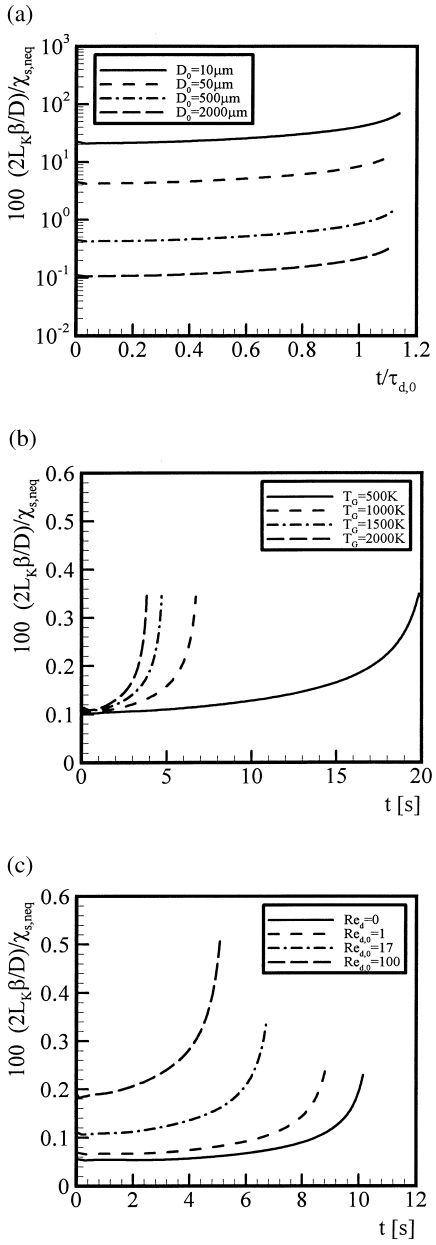

Fig. 7. Temporal evolution of the non-equilibrium contribution to the surface mole fraction for Langmuir–Knudsen model M7 for the base conditions of Fig. 4; i.e. decane (T_B = 447.7 K) with T_G = 1000 K, $T_{d,0}$ = 315 K, D_0 = 2 mm and $Re_{d,0}$ = 17: calculations end when $m_d = 0.01\, m_{d,0}$ and the results are for various (a) initial droplet diameters; (b) gas temperatures, and (c) initial droplet Reynolds numbers.

Fig. 8). If the quasi-steady analytical solution is used consistently for both mass and heat transfer for model M5, then the rapid mixing model M1 used in Fig. 8 is recovered. Furthermore, the unphysical attributes associated with absorbing the denominator of the

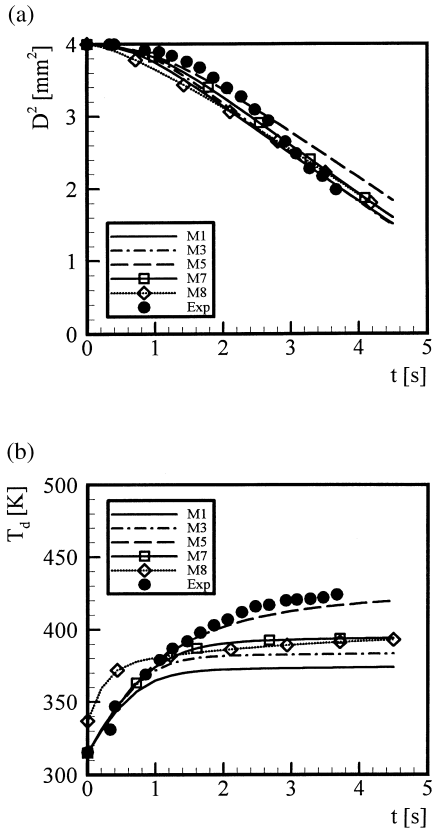

Fig. 8. Temporal evolution of the (a) droplet diameter squared and (b) the droplet temperature; for decane ($T_B = 447.7$ K) with various models modified to use the heat transfer reduction due to evaporation, $f_2 = G$. The experimental results are from Wong and Lin (1992) and the conditions are: $T_G = 1000$ K, $T_{d,0} = 315$ K, $D_0 = 2.0$ mm and $Re_{d,0} = 17$ (same as Fig. 4).

transfer number into the Sherwood number definition (as described in Section 2) are still present in model M5, and it cannot be recommended for use under more general conditions. Therefore, although several of the models perform well for the conditions of Fig. 8, the two Langmuir–Knudsen models must be recommended because non-equilibrium effects will be prevalent for many practical gas–liquid flows in which smaller droplets than currently investigated will be involved.

Given the analytical evaporative heat transfer correction $f_2 = G$, it is straightforward to show why the empirical f_2 corrections used in models M1–M6 fail to correctly capture the droplet evolution for high evaporation rates. Recall the commonly used empirical heat transfer relation in terms of the transfer number $f_2 = (1 + B_T)^{-\kappa}$ which was discussed in conjunction with [19]. Fig. 9 qualifies the relationship between this form for f_2 and the "exact" analytical parameter G by using a logarithmic correlation of the two functions obtained for steady state ($m_d = 0.1\, m_{d,0}$) conditions from the Langmuir–Knudsen model M7. Three methods of calculating the thermal transfer number are considered: (I) uses the definition of B_T from [8] used in this paper and also by Crowe et al. (1977), (II) is defined by the enthalpy difference,

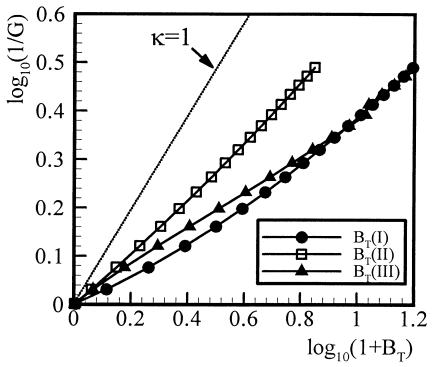

Fig. 9. Correlation of the steady state function G and the corresponding transfer numbers including several methods of calculating B_T (results are taken at $m_d = 0.1\, m_{d,0}$) for the Langmuir–Knudsen model M7. The fuel is decane with $T_{d,0} = 298$ K, $D_0 = 1$ mm and $U_G = 0$. The results are from 25 simulations calculated for $300\ \text{K} \leq T_G \leq 2000$ K in intervals of 100 K (from left to right).

$B_T = (C_{p,G}T_G - C_{p,s}T_d)/L_V$, suggested by Yuen and Chen (1978) with $\kappa = 1$ ($C_{p,s}$ is the surface heat capacity mass averaged with Y_s); and (III) corresponds to the definition of (I) except that the heat capacity is calculated using the "1/3 rule" defined by [23]–[26]. With this presentation, the "best" exponent κ for fitting the analytical relation is given by the slope of the curves. Note that the linearity of the curves is improved for methods (II) and (III); however, this occurs at the expense of evaluating the heat capacities at every numerical time step. For the present evaluations, models M1, M3 and M5 neglect evaporation effects ($\kappa = 0$), while models M4 and M6 implement the linear approximation $\kappa = 1$. Fig. 9 clearly shows that neither of these relations is capable of accurately modeling the "true" analytical solution for all but the smallest evaporation rates. Furthermore, while the non-linear proposals by Narashimhan and Gauvin (1967), and Renksizbulut and Yuen (1983) (having $\kappa = 2/3$ and $\kappa = 0.7$, respectively) provide very good approximations to G if method (II) is used, there is no need to use empirical expressions for f_2 with any of the models since the analytical functionality is known directly from the quasi-steady gas phase solution.

3.4. Effect of reference conditions for property evaluation

Since the method for evaluating thermophysical properties is still an unsettled subject, the reference temperature at which the constant properties are calculated in this study is evaluated. In Fig. 10 we display the decane data of Wong and Lin (1992) and compare it with the predictions of the Langmuir–Knudsen model M7 using several combinations of property reference conditions for both the vapor and the gas phase species (listed first and second in the legend, respectively). These include using the wet bulb, the boiling temperature, the time dependent "1/3 rule" and the ambient temperature for the carrier gas properties. All of the simulations use constant properties in time except for the "1/3 rule" defined by (23)–(26). The results show that using a reference temperature larger than the droplet surface temperature (i.e. T_G) results in a considerable over prediction of the experimental evaporation rate measurements. For the particular conditions of this experiment, the constant property methods

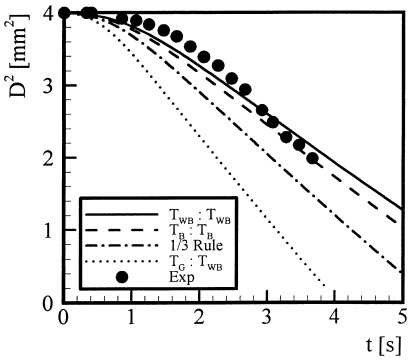

Fig. 10. Sensitivity of the droplet mass reduction predictions on the reference temperature used to evaluate the carrier gas (listed first in the legend) and vapor species constant properties. The results are for the Langmuir–Knudsen model M7 and the conditions and experimental data are the same as from Fig. 4; i.e. decane ($T_B = 447.7$ K) with $T_G = 1000$ K, $T_{d,0} = 315$ K, $D_0 = 2$ mm and $Re_{d,0} = 17$.

with T_{WB} and T_B provide more accurate predictions than the time dependent "1/3 rule" with a significant decrease in numerical complexity. However, for lower gas temperatures (lower evaporation rates) there may be a larger difference between the boiling and wet bulb conditions and the use of T_B may not be as accurate. The "1/3 rule" appears to most correctly capture the slope of the experimental data at late times; however, this method substantially overpredicts the initial transient decay rate during which the majority of the droplet mass is evaporated. Therefore, it is recommended that the constant property reference temperature should be taken as T_{WB} whenever possible, and as T_B when wet bulb estimates are unavailable. Note that the constant property approach described in this paper may not be appropriate when large deviations in T_G are present in the flow configuration.

3.5. Experiments of Chen et al. (1997)

We address here the issue of the experimental measurements and model predictions of Chen et al. (1997) for $\approx 55\,\mu$m decane and hexane droplets injected through a convective air environment with positive mean temperature and velocity gradients. Attempts to compare the present models to these experiments were unsuccessful, having large overpredictions of the measured D^2 reduction rates for all models, particularly for decane vaporization for which the experimental evaporation rate is nearly five times smaller than our model predictions (not shown). It was determined that this is a direct effect of inconsistencies between the measured and predicted evaporation rates, and not in the modeled droplet trajectories as calculated with (1), (2) and (5). However, the gas temperature in these experiments is relatively moderate (varying nearly linearly from approximately 370 K $\rightarrow$ 410 K along the 70 mm length of the chamber) and all Re_d are $\sim$1. These conditions are well within the range of parameters for which excellent agreement is found between the present Langmuir–Knudsen models and the results for both hexane (Fig. 3) and decane at a higher gas temperature (Fig. 4). Therefore, the only substantial difference for their experiments is the initial droplet size. Fig. 11 shows the time evolution of the droplet diameter squared for decane droplets of different initial sizes evaporating in quiescent air at 400 K (corresponding approximately to the largest experimental

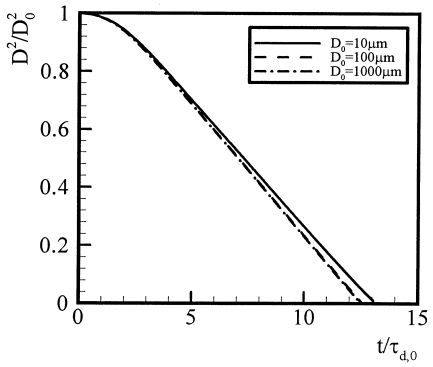

Fig. 11. Droplet diameter squared as a function of time normalized by the initial particle response time for the Langmuir–Knudsen model M7 for various initial droplet sizes. The fuel is decane and the simulation conditions are: $T_G = 400$ K, $T_{d,0} = 298$ K, and $U_G = 0$.

ambient temperature). The observed coincidence of all curves indicates that the small droplet sizes alone cannot explain the inability of the present models to capture the experimental trends (as expected, the "D^2 law" behavior is independent of the initial droplet size within this range of diameters).

Chen et al. (1997) also provide results obtained from three models, corresponding to the classical evaporation rate with: (1) infinite liquid conductivity (rapid mixing); (2) finite liquid conductivity; and (3) constant droplet temperature. Both of their models (1) and (2) are shown to agree well with the aforementioned experimental results. We were not able to reproduce their model predictions, even though their model (1) is identical to our model M1 except in the treatment of properties for which they use the method of Law and Williams (1972) with $A = 1/2$ (although we tried this method; see also Fig. 9). However, a thorough examination of the model used by Chen et al. (1997) (and also Chen, 1989) reveals that an *ad hoc* term of unstated magnitude is added into the correlation for latent heat as a function of temperature. As a final test used to settle this issue, we applied our numerical code using model M1 in an attempt to reproduce previous numerical results by Aggarwal *et al.* (1984), also using the same rapid mixing model, under nearly equivalent conditions (decane, $D_0 = 47.6\ \mu$m, $T_G = 1000$ K, $T_{d,0} = 300$ K, $Re_{d,0} = 0$ and 200). The only primary differences between these conditions and those of Chen et al. (1997) is that the pressure is now ten atmospheres (hence the saturation temperature is raised to 559.3 K) and there are no carrier gas temperature or velocity gradients (although the temperature and Reynolds numbers are substantially larger). Our results are in nearly perfect agreement with the rapid mixing results presented by Aggarwal *et al.* (1984) (not shown). Therefore, given both the ability of the present code to reproduce these simulation results for the same fuel and droplet size, and the additional broad predictive agreement documented in the present paper with a variety of other experiments (particularly for the Langmuir–Knudsen models), both the experimental data (which also shows the largest hexane evaporation rates at locations of smallest T_G) and the *ad hoc* modeling approach employed in Chen et al. (1997) (which has not been validated with other data) remain suspicious. Nevertheless, the questions raised by the disagreement between our results and those of Chen et al. (1997) remain unanswered (Switzer, 1997) and should be clarified in future studies.

4. Conclusions

An extensive evaluation of computationally efficient liquid droplet evaporation models available for use in many-droplet gas–liquid flow simulations is made through comparisons with a variety of experimental results. All comparisons are performed at atmospheric pressure, and for isolated single-component water, benzene, decane, heptane and hexane droplets vaporizing in uniform temperature air environments, under both quiescent and convective conditions. The models considered in this study include two forms of the classical "D^2 law" model which consider transient droplet heating effects: in one form the liquid thermal conductivity is assumed infinite, and in the other model Stefan flow effects are additionally included. Four versions of a simple heat–mass transfer analogy model are also considered, as well as two non-equilibrium Langmuir–Knudsen evaporation law formulations based on infinite liquid conductivity and finite liquid conductivity, respectively. All models are implemented by evaluating both the gas and vapor species properties only once, at the estimated wet bulb temperature, and assuming them to remain constant thereafter. Furthermore, the Langmuir–Knudsen law is shown to have a logarithmic form when combined with the quasi-steady analytical solutions of the gas phase field. With this formulation, the infinite liquid conductivity form of the model is no more computationally expensive than any of the other models considered in this paper. The finite conductivity version also does not require iteration, but involves the solution of an additional Lagrangian equation for the difference between the droplet surface temperature and its volume averaged temperature. This latter model does not yield significantly different results than the infinite conductivity version for the conditions of this study; however, it can be used when internal droplet temperature profiles are of interest.

Detailed comparisons for relatively large initial droplet sizes ($\sim$1 mm) indicate that the two non-equilibrium evaporation models agree most favorably with a wide range of experimental measurements for the temporal evolutions of both the droplet size and temperature. These improved predictions are apparent only when the gas temperature is either approximately equal to, or substantially larger than the liquid boiling point, yielding relatively moderate to large evaporation rates, respectively. For gas temperatures much lower than boiling, the evaporation rates are relatively small and all of the models yield nearly identical predictions in good agreement with the experimental results. The results reveal that thermodynamic non-equilibrium effects are important for initial droplet diameters $< 50\ \mu$m, but are nearly negligible for the experimental conditions under which the comparisons are made. Therefore, even though the Langmuir–Knudsen models considered here outperform the remaining models at high temperature, it is shown that, for large droplets, this improvement is not a direct consequence of non-equilibrium effects. A further analysis of the models shows that it is the analytic form for heat transfer reduction due to evaporation which is responsible for the improved performance of the present Langmuir–Knudsen models. This analytical form is obtained from the solution of the quasi-steady gas phase equations and can be used with any of the remaining models to substantially enhance their predictive capability. Nevertheless, it is argued that the Langmuir–Knudsen law should be used for general gas–liquid flow calculations because not only does it incorporate realistic non-equilibrium evaporation behavior prevailing

in many practical situations but also requires no more computational effort than the remaining models.

Acknowledgements

This research was conducted at the California Institute of Technology's Jet Propulsion Laboratory (JPL) and sponsored by General Electric (GE) through the Air Force Office of Scientific Research (AFOSR) Focused Research Initiative program with Dr David Burrus from GE serving as contract monitor. Computational resources were provided by the super computing facility at JPL.

Appendix A

The temperature dependent properties for the carrier gas and vapor species are required for the reference condition methods described in the text; however, all liquid properties are assumed constant. The properties are compiled from a variety of sources as indicated below, where the temperature is in degrees Kelvin and the pressure is in atmospheres. For species in which neither the diffusivity nor the Schmidt number are provided, it is assumed that the Lewis number is equal to unity and the diffusivity (Γ) is calculated with the density also evaluated at the reference temperature:

1. Air (Harpole, 1981):

$$W_C = 28.97 \text{ kg (kg mole)}^{-1},$$

$$\mu_C = 6.109 \times 10^{-6} + 4.604 \times 10^{-8} T - 1.051 \times 10^{-11} T^2 \text{ kg m}^{-1}\text{s}^{-1},$$

$$\lambda_C = 3.227 \times 10^{-3} + 8.3894 \times 10^{-5} T - 1.9858 \times 10^{-8} T^2 \text{ J m}^{-1} \text{ s}^{-1} \text{ K}^{-1},$$

$$Pr_C = 0.815 - 4.958 \times 10^{-4} T + 4.514 \times 10^{-7} T^2; \quad \text{for } T \leq 600 \text{ K},$$

$$Pr_C = 0.647 + 5.5 \times 10^{-5} T; \quad \text{for } T > 600 \text{ K}.$$

2. Benzene (Reid et al., 1987; Petroleum Refining Data Book, 1992):

$$W_V = 78.114 \text{ kg (kg mole)}^{-1},$$
$$T_B = 353.2 \text{ K},$$
$$C_{p,V} = 434.2 + 6.073T - 3.862 \times 10^{-3} T^2 \text{ J kg}^{-1} \text{ K}^{-1},$$
$$\mu_V = 6.2571 \times 10^{-6} + 7.166 \times 10^{-9} T \text{ kg m}^{-1} \text{ s}^{-1},$$
$$\lambda_V = 4.471 \times 10^{-3} + 5.606 \times 10^{-5} T + 2.773 \times 10^{-9} T^2 \text{ J m}^{-1} \text{ s}^{-1} \text{ K}^{-1},$$
$$\Gamma_V = 1.502 \times 10^{-10} (1.8T - 32)^{1.75} \text{ m}^2 \text{ s}^{-1},$$
$$L_V = 6.5120 \times 10^5 (1 - T/548.7)^{0.6775 - T/2036} \text{ J Kg}^{-1},$$
$$\rho_L = 810 \text{ Kg m}^{-3}$$
$$C_L = 1738 \text{ J kg}^{-1} \text{ K}^{-1},$$
$$\lambda_L = 0.1279 \text{ J m}^{-1} \text{ s}^{-1} \text{ K}^{-1}.$$

3. Decane ($T^* = T/1000$) (Abramzon and Sirignano, 1989):

$$W_V = 142 \text{ kg (kg mole)}^{-1},$$
$$T_B = 447.7 \text{ K},$$
$$C_{p,V} = 106.6 + 5765T^* - 1675T^{*2} + 473.1T^{*3} \text{ J kg}^{-1} \text{ K}^{-1} \quad \text{for } T^* \leq 0.8,$$
$$C_{p,V} = 411.1 + 5460T^* - 2483T^{*2} + 422.9T^{*3} \text{ J kg}^{-1} \text{ K}^{-1} \quad \text{for } T^* > 0.8,$$
$$\mu_V = 5.64 \times 10^{-6} + 1.75 \times 10^{-8} (T - 300) \text{ kg m}^{-1} \text{ s}^{-1},$$
$$\lambda_V = 1.214 \times 10^{-2} (T/300)^{1.8} \text{ J m}^{-1} \text{ s}^{-1} \text{ K}^{-1},$$
$$\Gamma_V = 5.46 \times 10^{-6} (T/300)^{1.583} P^{-1} \text{ m}^2 \text{ s}^{-1},$$
$$L_V = 3.958 \times 10^4 (619 - T)^{0.38} \text{ J Kg}^{-1},$$
$$\rho_L = 642 \text{ Kg m}^{-3}$$
$$C_L = 2520.5 \text{ J kg}^{-1} \text{ K}^{-1},$$
$$\lambda_L = 0.1055 \text{ J m}^{-1} \text{ s}^{-1} K^{-1}.$$

Heptane (Park and Aggarwal, 1995):

$$W_V = 100 \text{ kg (kg mole)}^{-1},$$
$$T_B = 371.6 \text{ K},$$
$$C_{p,V} = -51.56 + 6.776T - 3.658 \times 10^{-3}T^2 - 7.673 \times 10^{-7}T^3 \text{ J kg}^{-1} \text{ K}^{-1},$$
$$\mu_V = 3.83 \times 10^{-6} - 3.613 \times 10^{-9}T + 4.911 \times 10^{-11}T^2 - 3.577 \times 10^{-14}T^3 \text{ kg m}^{-1} \text{ s}^{-1},$$
$$\lambda_V = -4.401 \times 10^{-2} + 2.514 \times 10^{-4}T - 3.173 \times 10^{-7}T^2 + 2.487 \times 10^{-10}T^3 \text{ J m}^{-1} \text{ s}^{-1} \text{ K}^{-1},$$
$$\Gamma_V = 5.94 \times 10^{-6}(T/273)^{1.6} P^{-1} \text{ m}^2 \text{ s}^{-1},$$
$$L_V = 3.163 \times 10^5(3.204 - T/168.6)^{0.38} \text{ J Kg}^{-1},$$
$$\rho_L = 649.38 \text{ kg m}^{-3},$$
$$C_L = 2383.89 \text{ J kg}^{-1} \text{ K}^{-1},$$
$$\lambda_L = 0.1768 \text{ J m}^{-1} \text{ s}^{-1} \text{ K}^{-1}.$$

Hexane (Reid et al., 1987; Petroleum Refining Data Book, 1992):

$$W_V = 86.178 \text{ kg (kg mole)}^{-1},$$
$$T_B = 344.6 \text{ K},$$
$$C_{p,V} = -51.31 + 6.767T - 3.626 \times 10^{-3}T^2 \text{ J kg}^{-1} \text{ K}^{-1},$$
$$\mu_V = 5.592 \times 10^{-6} + 5.622 \times 10^{-9}T \text{ kg m}^{-1} \text{ s}^{-1},$$
$$\lambda_V = 1.112 \times 10^{-2} + 3.837 \times 10^{-5}T + 3.778 \times 10^{-8}T^2 \text{ J m}^{-1} \text{ s}^{-1} \text{ K}^{-1},$$
$$L_V = 5.1478 \times 10^5(1 - T/512)^{0.3861} \text{ J Kg}^{-1},$$
$$\rho_L = 664 \text{ kg m}^{-3},$$
$$C_L = 2302 \text{ J kg}^{-1} \text{ K}^{-1},$$
$$\lambda_L = 0.1046 \text{ J m}^{-1} \text{ s}^{-1} \text{ K}^{-1}.$$

Water (Harpole, 1981):

$$W_V = 18.015 \text{ kg (kg mole)}^{-1},$$
$$T_B = 373.15 \text{ K},$$
$$C_{p,V} = 8137 - 37.34T + 0.07482T^2 - 4.956 \times 10^{-5}T^3 \text{ J kg}^{-1} \text{ K}^{-1},$$
$$\mu_V = 4.07 \times 10^{-8}T - 3.077 \times 10^{-6} \text{ kg m}^{-1} \text{ s}^{-1},$$
$$\lambda_V = 1.024 \times 10^{-2} - 8.21 \times 10^{-6}T + 1.41 \times 10^{-7}T^2 - 4.51 \times 10^{-11}T^3 \text{ J m}^{-1} \text{ s}^{-1} \text{ K}^{-1},$$
$$L_V = 2.257 \times 10^6 + 2.595 \times 10^3(373.15 - T) \text{ J Kg}^{-1},$$
$$\rho_L = 997 \text{ kg m}^{-3},$$
$$C_L = 4184 \text{ J kg}^{-1} \text{ K}^{-1},$$
$$\lambda_L = 0.6531 \text{ J m}^{-1} \text{ s}^{-1}\text{K}^{-1}.$$

References

Abramzon, B., Sirignano, W.A., 1989. Droplet vaporization model for spray combustion calculations. Int. J. Heat Mass Transfer 32 (9), 1605–1618.

Aggarawal, S.K., Tong, A.Y., Sirignano, W.A., 1984. A comparison of vaproization models in spray calculations. AIAA J. 22 (10), 1448–1457.

Aggarwal, S.K., Peng, F., 1995. A review of droplet dynamics and vaporization modeling for engineering calculations. J. Eng. Gas Turbines Power 117, 453–461.

Bellan, J., Harstad, K., 1987a. Analysis of the convective evaporation of nondilute clusters of drops. Int. J. Heat Mass Transfer 30 (1), 125–136.

Bellan, J., Harstad, K., 1987b. The details of the convective evaporation of dense and dilute clusters of drops. Int. J. Heat Mass Transfer 30 (6), 1083–1093.

Bellan, J., Summerfield, M., 1978. Theoretical examination of assumptions commonly used for the gas phase surrounding a burning droplet. Comb. Flame 33, 107–122.

Berlemont, A., Grancher, M.S., Gouesbet, G., 1991. On the Lagrangian simulation of turbulence influence on droplet evaporation. Int. J. Heat Mass Transfer 34 (11), 2805–2812.

Bird, R.B., Stewart, W.E., Lightfoot, E.N. 1960. Transport Phenomena. Wiley, New York.

Chen, G. 1989. Vaporization behavior of pure and multicomponent fuel droplets in a hot air stream. Masters thesis, University of Illinois at Chicago, Department of Mechanical Engineering.

Chen, G., Aggarwal, S.K., Jackson, T.A., Switzer, G.L., 1997. Experimental study of pure and multicomponent fuel droplet evaporation in a heated air flow. Atom. Sprays 7, 317–337.

Chen, G., Mazumder, M., Chang, R.K., Swindal, J.C., Acker, W.P., 1996. Laser diagnostics for droplet characterization: application of morphology dependent resonances. Prog. Eng. Comb. Sci. 22, 163–188.

Chen, X.Q., Pereira, J.C.F., 1996. Computation of turbulent evaporating sprays with well-specified measurements: a sensitivity study on droplet properties. Int. J. Heat Mass Transfer 39 (3), 441–454.

Cliffe, K.A., Lever, D.A., 1985. Isothermal flow past a blowing sphere. Int. J. Numerical Methods Fluids 5, 709–725.

Crowe, C.T., Sharma, M.P., Stock, D.E., 1977. The particle source in cell (PSI-cell) model for gas-droplet flows. J. Fluids Eng. 6, 325–332.

Crowe, C.T., Troutt, T.R., Chung, J.N., 1996. Numerical models for two-phase turbulent flows. Ann. Rev. Fluid Mech. 28, 11–43.

Downing, C.G., 1966. The evaporation of drops of pure liquids at elevated temperatures: rates of evaporation and wet-bulb temperatures. AIChE J. 12 (4), 760–766.
Drew, D.A., Lahey, R.T., 1993. Analytical modeling of multiphase flow. Particulate Two Phase Flow. Roco MC, Ed., pp. 509–566.
Eaton, J.K., Fessler, J.R., 1994. Preferential concentration of particles by turbulence. Int. J. Multiphase Flow 20, 169–209.
Eisenklam, P., Arunachalam, S.A., Weston, J.A. 1953. Evaporation rates and drag resistance of burning drops. In: Proceedings of the Eleventh Symposium (International) on Combustion. Combustion Institute, Baltimore, MD, 715–727.
Godsave, G.A.E. 1953. Studies of the combustion of drops in a fuel spray: the burning of single drops of fuel. In: Proceedings of the Fourth Symposium (International) on Combusion. Combustion Institute, Baltimore, MD, 818–830.
Hanlon, T.R., Melton, L.A., 1992. Exciplex flourescence thermometry of falling hexadecane droplets. J. Heat Transfer 114, 450–457.
Harpole, G.M., 1981. Droplet evaporation in high temperature environments. J. Heat Transfer 103, 86–91.
Harstad, K., Bellan, J., 1991. A model of the evaporation of binary-fuel clusters of drops. Atom. Sprays 1, 367–388.
Hubbard, G.L., Denny, V.E., Mils, A.F., 1975. Droplet evaporation: effects of transients and variable properties. Int. J. Heat Mass Transfer 18, 1003–1008.
Jackson, R., Davidson, B.J., 1983. An equation set for non-equilibrium two phase flow, and an analysis of some aspects of choking, acoustic propagation, and losses in low pressure wet steam. Int. J. Multiphase Flow 9 (5), 491–510.
Kassoy, D.R., Williams, F.A., 1968. Variable property effects on liquid droplet combustion. AIAA J. 6(10), 1961–1965.
Law, C.K., Law, H.K., 1976. Quasi-steady diffusion flame theory with variable specifc heats and transport coefficients. Comb. Sci. Tech. 12, 207–216.
Law, C.K., Williams, F.A., 1972. Kinetics and convection in the combustion of alkane droplets. Comb. Flame 19, 393–405.
Mashayek, F. 1998a. Direct numerical simulations of evaporating droplet dispersion in forced low Mach number turbulence. Int. J. Heat Mass Transfer. 41(17), 2601–2617.
Mashayek, F. 1998b. Droplet-turbulence interactions in low Mach number homogeneous shear two-phase flows. J. Fluid Mech. 376, 163–203.
Mashayek, F., Jaberi, F.A., Miller, R.S., Givi, P., 1997. Dispersion and polydispersity of droplets in stationary isotropic turbulence. Int. J. Multiphase Flow 23 (2), 337–355.
Narashimhan, C., Gauvin, W.H. 1967. Heat and mass transfer to spheres in high temperature surroundings. Can. J. Chem. Eng. 45. 181–188. .
Park, T.W., Aggaral, S.K. 1995. Gravity effects on the dynamics of evaporating droplets in a heated jet. J. Propulsion Power. 11(3) 519–528. .
Petroleum, Refining. 1992. Technical report. vols. 2,3. American Petroleum Institution, Washington, D.C.
Ranz, W.E., Marshall, W.R. 1952a. Evaporation from drops: I. Chem. Engng. Prog. 48. 141–146.
Ranz, W.E., Marshall, W.R. 1952b. Evaporation from drops: II. Chem. Engng. Prog. 48. 173–180.
Reid, R.C., Prausnitz, J.M., Poling, B.E. 1987. The Properties of Gases and Liquids. McGraw–Hill, New York.
Renksizbulut, M., Haywood, R.J., 1988. Transient droplet evaporation with variable properties and internal circulation at intermediate Reynolds numbers. Int. J. Multiphase Flow 14 (2), 189–202.
Renksizbulut, M., Yuen, M.C., 1983. Experimental study of droplet evaporation in a high temperature air stream. J. Heat Transfer 105, 384–388.
Sirignano, W.A., 1993. Fluid dynamics of sprays. J. Fluids Eng. 115, 345–378.
Spalding, D.B. 1953a. The combustion of liquid fuels. In: Proceedings of the Fourth Symposium (International) on Combustion. Combustion Institute, Baltimore, MD, 847–864. .
Spalding, D.B. 1953b. Experiments on the burning and extinction of liquid fuel spheres. Fuel. 32, 169–185.
Swindal, J.C., Chen, G., Scheschak, K., Chang, R.K., Jackson, T., 1996. Measurement of the evaporation rates of closely spaced flowing droplets by optical cavity resonances. Atom. Sprays 6, 331–351.
Switzer, G.L. 1997. Personal communcation.
Tong, A.Y., Sirignano, W.A., 1982. Transient thermal boundary layer in heating of droplet with internal circulation: evaluation of assumptions. Comb. Sci. Tech. 29, 87–94.
Wells, M.R., Melton, L.A., 1990. Temperature measurements of falling droplets. J. Heat Transfer 112, 1008–1013.
Williams, F.A. 1965. Combustion Theory. Addison Wesley, Reading.
Wong, S.C., Lin, A.R., 1992. Internal temperature distributions of droplets vaporizing in high-temperature convective flows. J. Fluid Mech. 237, 671–687.
Yuen, M.C., Chen, L.W., 1976. On drag of evaporating liquid droplets. Comb. Sci. Tech. 14, 147–154.
Yuen, M.C., Chen, L.W., 1978. Heat-transfer measurements of evaporating liquid droplets. Int. J. Heat Mass Transfer 21, 537–542.